Stiffness Analysis of a New Tensegrity Mechanism Based on Planar Dual-triangles

Wanda Zhao, Anatol Pashkevich, Alexandr Klimchik, Damien Chablat

Stiffness Analysis of a New Tensegrity Mechanism Based on Planar Dual-triangles

Wanda Zhao[1], Anatol Pashkevich[1,2] Alexandr Klimchik[3] and Damien Chablat[1,4]
[1]*Laboratoire des Sciences du Numérique de Nantes (LS2N), UMR CNRS 6004, 1 rue de la Noe, 44321 Nantes, France*
[2]*IMT Atlantique Nantes, 4 rue Alfred-Kastler, Nantes 44307, France*
[3]*Innopolis University, Universitetskaya St, 1, Innopolis, Tatarstan, 420500, Russia*
[4]*Centre National de la Recherche Scientifique (CNRS), France*

Keywords: Tensegrity mechanisms, Equilibrium configurations, Stability analysis, Stiffness analysis.

Abstract: The paper deals with the stiffness analysis and stability study of a new type of tensegrity mechanism based on dual-triangle structures, which actuated by adjusting elastic connections between the triangle edges. For a single segment of such mechanism, the torque-deflection relation was obtained as a function of control inputs and geometric parameters. It was proved that a single section of the mechanism can has either a single or three equilibrium configurations that can be both stable and unstable. Corresponding conditions of stability were found allowing user to choose control inputs ensuring the mechanism controllability, and the obtained results are confirmed by the simulation examples. The structure composed of two segments in serial was also analysed and an equivalent serial structure with non-linear virtual springs in the joints was proposed. It was proved that the stiffness of such structure decreases while the external loading increases, which may lead to the buckling phenomenon.

1 INTRODUCTION

Many modern robotic applications require new type of manipulators that possess high flexibility similar to an elephant trunk (Rolf, M., Steil, J. J. 2012), (Yang, Y., Zhang, W. 2015). Such manipulators are usually composed of a number of similar segments based on varies tensegrity mechanisms, which are assembly of compressive elements and tensile elements (cables or springs) held together in equilibrium (Skelton, R. E., de Oliveira, M. C. 2009), (Moored, K. W., Kemp, T. H. et al. 2011). This paper concentrates on the stiffness analysis and equilibrium stability of a new type of tensegrity mechanism composed of two rigid triangle parts, which are connected by a passive joint in the centre and two elastic edges on each sides with controllable preload.

Some kinds of the tensegrity mechanisms have been already studied carefully in literature (Duffy, J., Rooney, J. et al. 2000), (Arsenault, M., Gosselin, C. M. 2006). In particular, the cable-driven X-shape tensegrity structures were considered in (Furet, M., Lettl, M., et al. 2018), (Furet, M., Wenger, P. 2018), where each section was composed of four fixed-length rigid bars and two springs. For this mechanism, the authors investigated influence on the cable lengths on the mechanism equilibrium configurations, which maybe both stable and unstable. Special attention was paid to the work space and singularities analysis. Another group of related works (Arsenault, M., Gosselin, C. M. 2006) deals with the mechanism composed of two springs and two length-changeable bars. The authors analysed the mechanism stiffness using the energy method, and demonstrated that the stiffness of this mechanism always decreases when it is subjected to external loads with the actuators locked, which may lead to "buckling". Some other research in this area (Wenger, P., Chablat, D. 2018) focus on the three-spring mechanisms, for which the equilibrium configurations stability and singularity were analysed. Using these results the authors obtained conditions under which the mechanism can work continuously, without the "buckling" or "jump" phenomenon. There are also some research studying a four-legged parallel platform (Moon, Y., Crane, C. D., et al 2012), which is based on the compliant tensegrity mechanisms. Here, each leg consists of a piston and a spring in series, which allows the platform to achieve in the desired position and orientation. The authors investigated the loaded

equilibrium configurations and numerically computed the platform stiffness. However, the tensegrity mechanism based on dual-triangles were not studied in robotic literature yet.

This paper focuses on the stiffness analysis of a new tensegrity mechanism, which is based on rigid dual-triangles connected by a passive joint that is actuated by adjusting elastic connections between the remaining triangle edges. This structure is proved to be very promising for designing of multi-section series chain possessing very high flexibility. For this mechanism, we concentrate on the equilibriums computing, the stability analysis and the selection of the geometric parameters and control inputs allowing to achieve the desired configuration while ensuring its stability. The loaded and unloaded stiffness analysis of two-segments structure were also carried out in detail. The results provide a good base of the study of the multi-segment manipulators in the future work.

2 GEOMETRY ANALYSIS AND EQUILIBRIUM EQUATION

Let us consider first a 1-d.o.f. segment of the total flexible structure to be studied, which consists of two rigid triangles connected by a passive joint whose rotation is constrained by two linear springs as shown in Fig. 1. It is assumed that the mechanism geometry is described by the triangle parameters (a_1,b_1) and (a_2,b_2) , and the mechanism shape is defined by the angle that can be adjusted by means of two control inputs influencing on the spring lengths L_1 and L_2. Let us denote the spring lengths in the non-stress state as L_1^0 and L_2^0, and the springs stiffness coefficients k_1 and k_2.

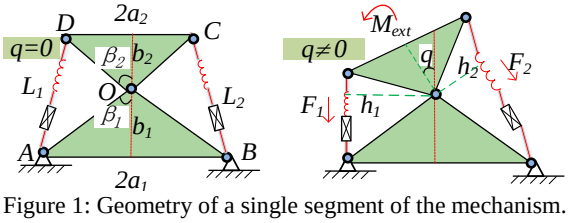

Figure 1: Geometry of a single segment of the mechanism.

To find mechanism configuration angle q corresponding to given control inputs L_1^0 and L_2^0, let us derive the static equilibrium equation. The forces F_1, F_2 generated by the springs can be obtained from Hook's law as follows.

$$F_1 = k_1 (L_1 - L_1^0); \quad F_2 = k_2 (L_2 - L_2^0) \tag{1}$$

where L_1 and L_2 are the spring lengths $|AD|$, $|BC|$ corresponding to the current value of the angle q. These values can be computed from the triangles ΔAOD and ΔBOC using the formulas

$$\begin{aligned} L_1(\theta_1) &= \sqrt{c_1^2 + c_2^2 + 2c_1c_2\cos(\theta_1)} \\ L_2(\theta_2) &= \sqrt{c_1^2 + c_2^2 + 2c_1c_2\cos(\theta_2)} \end{aligned} \tag{2}$$

where $c_1 = \sqrt{a_1^2 + b_1^2}$, $c_2 = \sqrt{a_2^2 + b_2^2}$ and θ_1, θ_2 are expressed via the mechanism parameters $\theta_1 = \beta_{12} + q$; $\theta_2 = \beta_{12} - q$; $\beta_{12} = \text{atan}(a_1 / b_1) + \text{atan}(a_2 / b_2)$.

The torques $M_1 = F_1 \cdot h_1$, $M_2 = -F_2 \cdot h_2$ created by the forces F_1, F_2 in the passive joint O can be computed using the triangle area relations $L_1 h_1 = c_1 c_2 \sin(\theta_1)$, $L_2 h_2 = c_1 c_2 \sin(\theta_2)$ of ΔAOD and ΔBOC, which yield the following expressions

$$\begin{aligned} M_1(q) &= +k_1 (1 - L_1^0 / L_1(\theta_1))\, c_1 c_2 \sin(\theta_1) \\ M_2(q) &= -k_2 (1 - L_2^0 / L_2(\theta_2))\, c_1 c_2 \sin(\theta_2) \end{aligned} \tag{3}$$

where the difference in signs is caused by the different direction of the torques generated by the forces F_1, F_2 with respect to the passive joint.

Further, taking into account the external torque M_{ext} applied to the moving platform, the static equilibrium equation for the considered mechanism can be written as follows

$$M_1(q) + M_2(q) + M_{ext} = 0 \tag{4}$$

Solving this equation we can get the rotation angle q_0 corresponding to the control inputs L_1^0, L_2^0 and the external torque M_{ext} applied to the moving platform. This equation is highly nonlinear and cannot be solved analytically, so it is reasonable to apply the numerical Newton technique, which leads to the iterative scheme

$$q^{k+1} = q^k - \left(M(q^k) + M_{ext}\right) / M'(q^k) \tag{5}$$

where $M(q) = M_1(q) + M_2(q)$, $M'(q^k) = dM(q)/dq$.

3 STABILITY ANALYSIS OF A SINGLE SEGMENT

Let us now evaluate the stability of the mechanism under consideration, which shows its controllability in relation to the external load. This property highly depends on the equilibrium configuration defined by the angle q satisfying the equilibrium equation $M(q)+M_{ext}=0$. As follows from the relevant analysis, the function $M(q)$ can be either monotonic or non-monotonic one, so the mechanism under study may have multiple stable and unstable equilibriums, which are studied in detail below.

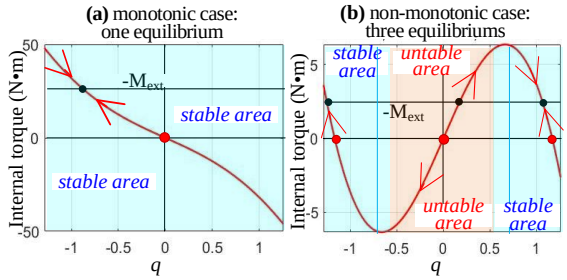

Figure 2: The torque-angle curves and equilibriums for different combinations of mechanism parameters.

To analyse the mechanism equilibriums, let us consider the torque-angle curves $M(q)=M_1(q)+M_2(q)$ defined by Eq. 3 and presented in Fig. 2. It is clear from Fig. 2a that for the monotonic function $M(q)$ with negative derivative, the increase of the external loading always leads to higher mechanism resistance, so the equilibrium is unique and stable. However, in the non-monotonic case, while increasing the external loading, it is possible to achieve a point where the mechanism does not resist any more and suddenly changes its configuration as shown in Fig. 2b. It is worth mentioning that similar phenomenon can be observed in other mechanism and is known in mechanics as "buckling" (Jones, R. M.). Hence, in the non-monotonic case, there maybe three solutions of the equilibrium equation (two stables and one unstable).

As follows from the above presented figures, the static equilibrium defined by angle q is stable if and only if the corresponding derivative $M'(q)$ is negative. However, taking into account possible shapes of the torque-angle curves $M(q)$ that can be either monotonic or two-model one, the considered stability condition can be simplified and reduced to the derivative sign verification at the zero point only, i.e.

$$M'(q)\big|_{q=0}<0 \tag{6}$$

and it is easy to verify in practice. It should be noted that here the derivative represent the mechanism stiffness for the unloaded configuration.

To compute the desired derivative for any given q, it is convenient to represent the function $M(q)$ in the following way

$$\begin{aligned} M(q)=c_1c_2k_1\sin\theta_1\left(1-L_1^0/L_1(\theta_1)\right)- \\ -c_1c_2k_2\sin\theta_2\left(1-L_2^0/L_2(\theta_2)\right) \end{aligned} \tag{7}$$

This allows us to express the mechanism stiffness in general case as follows

$$\begin{aligned} M'(q)=c_1c_2k_1\cos\theta_1\left(1-L_1^0/L_1(\theta_1)\right)+ \\ +c_1c_2k_2\cos\theta_2\left(1-L_2^0/L_2(\theta_2)\right)- \\ -c_1^2c_2^2k_1L_1^0\sin^2\theta_1/\left(L_1(\theta_1)\right)^3-c_1^2c_2^2k_2L_2^0\sin^2\theta_2/\left(L_2(\theta_2)\right)^3 \end{aligned} \tag{8}$$

For the special cases, when $q=0$ and $q=\beta_{12}$ (or $q=-\beta_{12}$), the above expression is simplified respectively to

$$\begin{aligned} M'(q)\big|_{q=0}=-c_1^2c_2^2\sin^2\beta_{12}\left(k_1L_1^0+k_2L_2^0\right)/\left(L(\beta_{12})\right)^3 \\ +c_1c_2\cos\beta_{12}\left[k_1+k_2-(k_1L_1^0+k_2L_2^0)/L(\beta_{12})\right] \end{aligned} \tag{9}$$

$$\begin{aligned} M'(q)\big|_{q_0=\beta_{12}}=c_1c_2k_1\cos2\beta_{12}\left[1-L_1^0/L(2\beta_{12})\right] \\ +c_1c_2k_2\left[1-L_2^0/(c_1+c_2)\right]-c_1^2c_2^2k_1L_1^0\sin^2 2\beta_{12}/\left(L\ (2\beta_{12})\right)^3 \end{aligned} \tag{10}$$

where $L\ (\beta_{12})=\sqrt{c_1^2+c_2^2+2c_1c_2\cos\beta_{12}}$,

$L\ (2\beta_{12})=\sqrt{c_1^2+c_2^2+2c_1c_2\cos2\beta_{12}}$.

Let us also consider in detail the symmetrical case, for which $a_1=a_2$, $b_1=b_2$, $c_1=c_2$, $k_1=k_2$, $L_1^0=L_2^0$. In this case, we can omit some indices and present the torque-angle relationship as well as the stiffness expression in forms that are more compact

$$M(q)=2ck\left(c\cos\beta_{12}\sin q-L^0\cos\frac{\beta_{12}}{2}\sin\frac{q}{2}\right) \tag{11}$$

$$M'(q)=ck\left(2c\cos\beta_{12}\cos q-L^0\cos\frac{\beta_{12}}{2}\cos\frac{q}{2}\right) \quad (12)$$

where the control input must satisfy the condition $0<L^0<2b$, as follows from the mechanism geometry (Fig. 1). To distinguish the monotonic and non-monotonic cases presented in Fig. 2, let us compute the derivative for the unloaded equilibrium

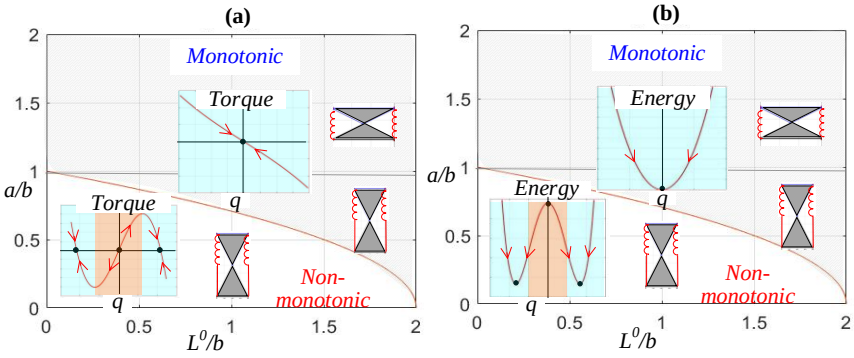

Figure 3: Stable and unstable regions of the parameter plane for unloaded equilibrium q = 0.

configuration $q=0$, which after simplification can be expressed in the following way

$$M'(q)\big|_{q=0}=k\left[2\left(b^2-a^2\right)-L^0b\right] \quad (13)$$

The latter allows us to present the condition (6) of torque-angle curve monotonicity as

$$\frac{L^0}{b}>2\left(1-\left(\frac{a}{b}\right)^2\right) \quad (14)$$

and separate the parameter plane in two regions as shown in Fig. 3a. As follows from this figure, the unloaded equilibrium is always stable if $a>b$. Otherwise, to have stable unloaded equilibrium, the control input $L_1^o=L_2^o$ should be higher than

$$L_i^o>2b\left[1-(a/b)^2\right];\ \ i=1,2$$

The monotonic and non-monotonic cases are also illustrated by Fig. 3b, which includes the energy curves

$$E(q)=\frac{1}{2}\sum_{i=1}^{2}k\left(L_i(q)-L^0\right)^2$$

as the function of the rotation angle q. As follows from this figure, the energy $E(q)$ has either a single minimum $q=0$ corresponding to a stable equilibrium, or two symmetrical minima

$$q_e=\pm 2\arccos\left(\frac{L^0b}{2\left(b^2-a^2\right)}\right) \quad (15)$$

and a local maximum $q=0$ corresponding to two stable equilibriums and one unstable equilibrium.

For the symmetrical case, where $L_1^0=L_2^0$, let us also compute the torques at the boundary points $q=\pm\beta_{12}$

$$M(q)\big|_{q=\pm\beta_{12}}=\pm\frac{2abk}{a^2+b^2}\left[2\left(b^2-a^2\right)-L^0c\right] \quad (16)$$

which allows us to present the condition that in the non-monotonic case the stable equilibriums are located inside of the interval of feasible values of the configuration variable $|q_e|<|\beta_{12}|$:

$$L^0>\frac{2\left(b^2-a^2\right)}{\sqrt{b^2+a^2}} \quad (17)$$

and allows user to estimate if the energy minimum is achieved inside or on the border of the feasible region of q. A physical interpretation of this equation is shown in Fig. 4. where two cases are presented. In the first case, the mechanism is unstable in the desired configuration $q=0$ and jumps to one of two possible stable configurations $q=\pm\beta_{12}$ that are located inside of mechanical limits. In the second case, the mechanism is also unstable in the equilibrium configuration $q=0$ but it jumps to one of the mechanical limits $q=\pm\beta_{12}$ (because the stable configurations are out of the

limits). So, a static error appears in both cases, where q is equal to either $\pm\beta_{12}$ or $\pm q_e$. For this reason, it is necessary to avoid in practice the parameters combinations producing non-monotonic torque-angle curves.

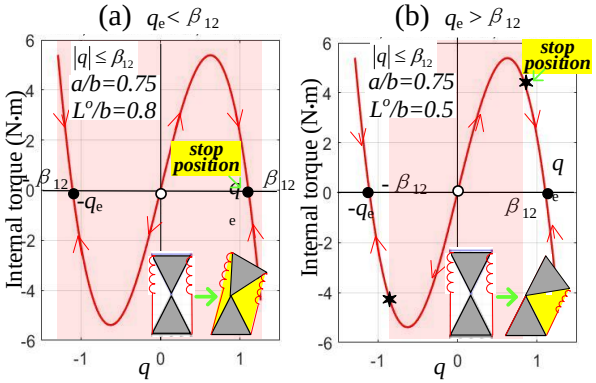

Figure 4: Location of stable "●" and unstable "o" equilibriums with respect to geometric boundary $[-\beta_{12}, \beta_{12}]$

It is also useful to investigate the case when the control inputs are not equal, i.e. $L_1^0 \neq L_2^0$, assuming that they produce the desired stable configuration with the output angle $q \neq 0$. In this case, the torque and its derivative can be presented as follows.

$$M(q) = 2c^2 k \cos\beta_{12} \sin q - \\ -ck\left[L_1^0 \sin\frac{\beta_{12}+q}{2} - L_2^0 \sin\frac{\beta_{12}-q}{2}\right] \quad (18)$$

$$M'(q) = 2k\left(b^2 - a^2\right)\cos q - \\ -0.5k\left[b\cos(q/2)(L_1^0 + L_2^0) - a\sin(q/2)(L_1^0 - L_2^0)\right] \quad (19)$$

where all notations are the same as in the above expressions (7) and (8). It can be proved from the equilibrium equation that the control inputs L_1^0, L_2^0 insuring the desired output angle q must satisfy the linear relation

$$L_1^0 \sin\frac{\beta_{12}+q}{2} - L_2^0 \sin\frac{\beta_{12}-q}{2} = 2c\cos\beta_{12}\sin q \quad (20)$$

which gives infinite set of control variables $\left\{L_1^0, L_2^0\right\}$ that may correspond either to stable or unstable equilibrium. To analyse sign of the derivative $dM(q)/dq$, let us consider separately two cases: $a > b$ and $a < b$. In the first case, when $a > b$ and mechanism geometry impose the constraint $|q| < \pi/2$, all three terms of (19) are negative, so the desired equilibrium configuration q is stable.

In the second case, when $a < b$, the equilibrium maybe either stable or unstable. Corresponding separation curves can be found from the conditions $M(q) = 0$ and $dM(q)/dq = 0$, which yield the following system of linear equations with respect to L_1^0, L_2^0

$$\left(\sin\frac{\beta_{12}+q}{2}\right)L_1^0 - \left(\sin\frac{\beta_{12}-q}{2}\right)L_2^0 = 2c\cos\beta_{12}\sin q \quad (21)$$

$$\left(a\sin\frac{q}{2} - b\cos\frac{q}{2}\right)L_1^0 - \left(a\sin\frac{q}{2} + b\cos\frac{q}{2}\right)L_2^0 = \\ = -4\left(b^2 - a^2\right)\cos q \quad (22)$$

whose solution allows us to present the stability condition in the following form

$$\frac{L_1^0}{b} > 2\left(\frac{b}{a} - \frac{a}{b}\right)\left(\frac{a}{b}\cos^3\frac{q}{2} + \sin^3\frac{q}{2}\right) \\ \frac{L_2^0}{b} > 2\left(\frac{b}{a} - \frac{a}{b}\right)\left(\frac{a}{b}\cos^3\frac{q}{2} - \sin^3\frac{q}{2}\right) \quad (23)$$

It is worth mentioning that in the case of $q = 0$ the above expressions give the stability condition Eq. 23.

Hence, to achieve the desired configuration q it is necessary to apply the control inputs L_1^0, L_2^0 satisfying both the equilibrium condition Eq. 21 and the stability conditions Eq. 22. Corresponding regions of L_1^0, L_2^0 are presented in Fig. 5, which clearly shows for which combination of inputs the desired configuration can be reached geometrically and it is statically stable, and where the angle q is constrained by the geometry conditions:

$$|q| < 2\text{atan}(a/b), \quad a \le b$$
$$|q| < \pi - 2\text{atan}(a/b), \quad a > b \qquad (24)$$

which allows us to get the value of q_{Max} in Fig. 5.

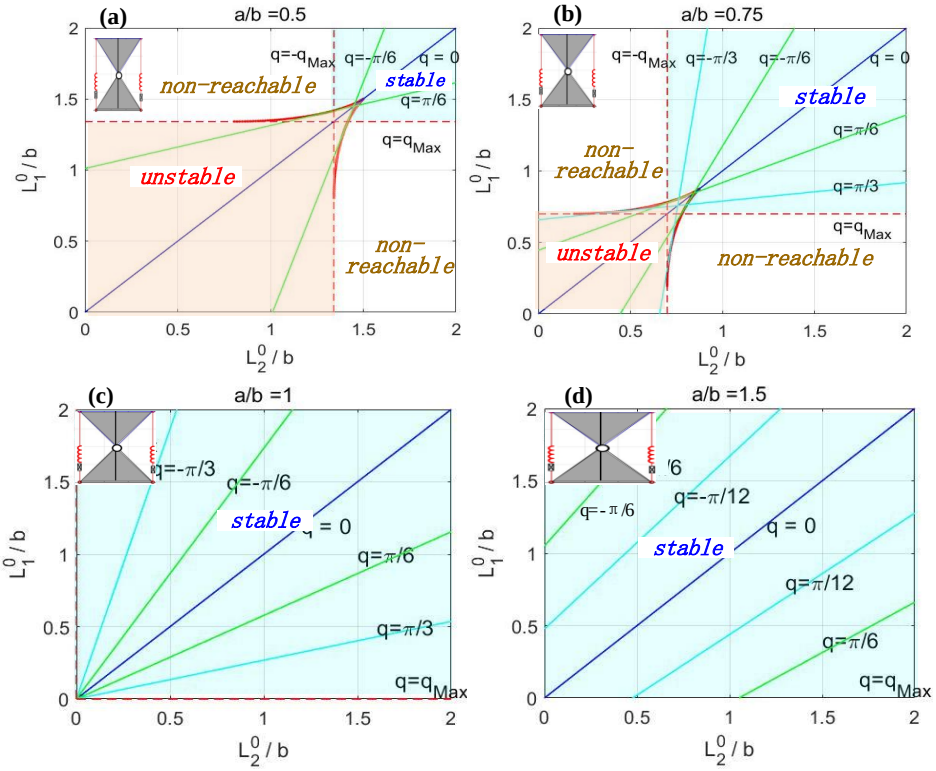

Figure 5: Regions of equilibrium stability for different inputs L_1^0, L_2^0.

4 STABILITY ANALYSIS OF TWO SEGMENTS

Let us consider now an aggregated mechanism presented in Fig. 6, which is composed of two segments considered in the previous section. It is assumed that the left hand-side of the mechanism is fixed and the desired configuration corresponds to the "straight" shape with $q_1 = q_2 = 0$ that is achieved by applying equal control inputs to all segments. Under the influence of the external force F_e, the end-effector moves to a new equilibrium with the end-effector location $(x, y)^T = (4b - \delta_x, \delta_y)^T$ and nonzero configuration variables (q_1, q_2). Let us evaluate the mechanism resistance to the external force F_e for this "straight" configuration expressed by the force-deflection relation $F_e(\delta_x, \delta_y)$.

If the end-effector deflection (δ_x, δ_y) is assumed to be known, the configuration angles can be computed from the triangle equations

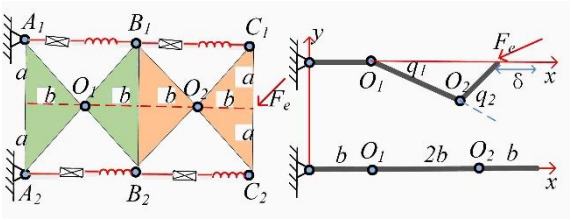

Figure 6: The model of two segment mechanism.

$$b + 2bC_1 + bC_{12} = 4b - \delta_x$$
$$2bS_1 + bS_{12} = \delta_y \qquad (25)$$

that can be solved using the technic used in the invers kinematics of the two-link manipulator, which yields

$$q_1 = \text{atan2}(y, x-b) - \text{atan2}\left(bS_2, 2b + bC_2\right)$$
$$q_2 = \text{atan2}\left(S_2, C_2\right) \quad (26)$$

where $C_2 = \left(\left(x-b\right)^2 + y^2 - 5b^2\right) \Big/ 4b^2$, $S_2 = \pm\sqrt{1-C_2^2}$. It is worth mentioning that two symmetrical solutions are possible here and both of them are feasible. Then, for each segment the torque generated by the elastic virtual spring can be obtained by Eq. 12

$$M\left(q_i\right) = 2k\left[\left(b^2 - a^2\right)\sin q_i - bL^o \sin\frac{q_i}{2}\right], \; i = 1, 2 \quad (27)$$

And we can get the relation between the torque $M\left(q_i\right)$ and the external force $\left(F_x, F_y\right)^T$

$$\begin{bmatrix} M\left(q_1\right) \\ M\left(q_2\right) \end{bmatrix} + J_q^T \begin{pmatrix} F_x \\ F_y \end{pmatrix} = 0 \quad (28)$$

where J_q is the Jacobian matrix, which is written as follows

$$J_q = \begin{bmatrix} -2bS_1 - bS_{1,2} & -bS_{1,2} \\ 2bC_1 + bC_{1,2} & bC_{1,2} \end{bmatrix} \quad (29)$$

and $C_1 = \cos q_1$, $S_1 = \sin q_1$, $C_{12} = \cos\left(q_1 + q_2\right)$, $S_{12} = \sin\left(q_1 + q_2\right)$. After substitution of the torques in the equilibrium equation, we can find the external force corresponding to the end-effector displacement

$$\begin{pmatrix} F_x \\ F_y \end{pmatrix} = 2kJ_q^{-T} \begin{bmatrix} -\sin q_1 & \sin\left(q_1/2\right) \\ -\sin q_2 & \sin\left(q_2/2\right) \end{bmatrix} \begin{bmatrix} b^2 - a^2 \\ bL^0 \end{bmatrix}, \; \left(q_2 \neq 0\right) \quad (30)$$

allowing us to obtain the desired force-deflection relation, which is presented in Fig. 7. These results show that the mechanism stiffness under external loading can be considered as nearly constant but the quasi-linear force-deflection curve does not go through the zero point. Also, the considered mechanism possesses very specific particularity leading to the buckling phenomenon when the external force increases gradually and the mechanism configuration angles suddenly change from zero to non-zero values. To find the critical force for the buckling, let us compute the limits of $\left(F_x, F_y\right)$ while $\left(\delta x, \delta y\right) \to (0, 0)$. As follows from the mechanism geometry, which include a triangle with edges size of b and $2b$, if the first angle $q_1 = \varepsilon$ is small enough, the second angle can be approximately expressed as $q_2 \approx -3\varepsilon$. The later allows us to express the Jacobian in the following form

$$J_q \approx \begin{bmatrix} 0 & 2b\varepsilon \\ 3b & b \end{bmatrix} \quad (31)$$

and rewrite equation (30) as

$$\begin{pmatrix} F_x \\ F_y \end{pmatrix} \approx 2k \cdot \begin{bmatrix} 0 & 2b\varepsilon \\ 3b & b \end{bmatrix}^{-T} \begin{bmatrix} -\varepsilon & \varepsilon/2 \\ 3\varepsilon & -3\varepsilon/2 \end{bmatrix} \begin{bmatrix} b^2 - a^2 \\ bL^0 \end{bmatrix} \quad (32)$$

that gives us the desired critical force

$$F_x^0 = \lim_{\varepsilon \to 0} F_x\left(\varepsilon\right) = 5k\left[2\left(b^2 - a^2\right) - bL^0\right] \Big/ 3b \quad (33)$$

It should also be mentioned that the buckling phenomenon occurs if $L^0/b > 2\left(1 - a^2/b^2\right)$, which in the previous section was recognized as the boundary condition separating the monotonic and non-monotonic areas in Fig. 3 (see in Eq. 15). Here, the initial configuration is stable and it resists to the external loading if $F_x < F_x^0$. In contrast, if the geometry satisfies the condition: $L^0/b < 2\left(1 - a^2/b^2\right)$ as shown in Fig. 7c, the initial configuration is unstable and the mechanism suddenly jumps from the initial position to slightly different stable equilibriums (even without external loading), which can be treated as the "jumping" phenomenon.

To get the unloaded stiffness matrix of the mechanism for the general case, let us assume that $q_1, q_2 \neq 0$ and the Jacobian is non-singular. This assumption allows us to apply an expression derived from the VJM method for the stiffness analysis of serial robots

$$\begin{pmatrix} F_x \\ F_y \end{pmatrix} = -J_q^{-T} K_q J_q^{-1} \begin{pmatrix} \delta x \\ \delta y \end{pmatrix} \quad (34)$$

where the diagonal matrix $K_q = diag(K_{q1}, K_{q2})$ is composed of the stiffness coefficient of virtual joint described by Eq. 13. This allows us to compute the unloaded stiffness matrix for the two-segment mechanism for any given configuration. Let us consider now the case when the end-effector is located at the point (δ_x, δ_y) assuming that $\delta_y = 0$. Corresponding configuration angles (q_1, q_2) can be computed from Eq. 26 and substituted further to the stable equilibrium condition (Eq. 19) for each segment of the mechanism. The latter also allows us to find equivalent stiffness coefficients

$K_{qi} = dM(q_i)/dq_i$ of the virtual joints. Then, the stiffness matrix of the two-segment mechanism can be obtained from the VJM method and expressed as

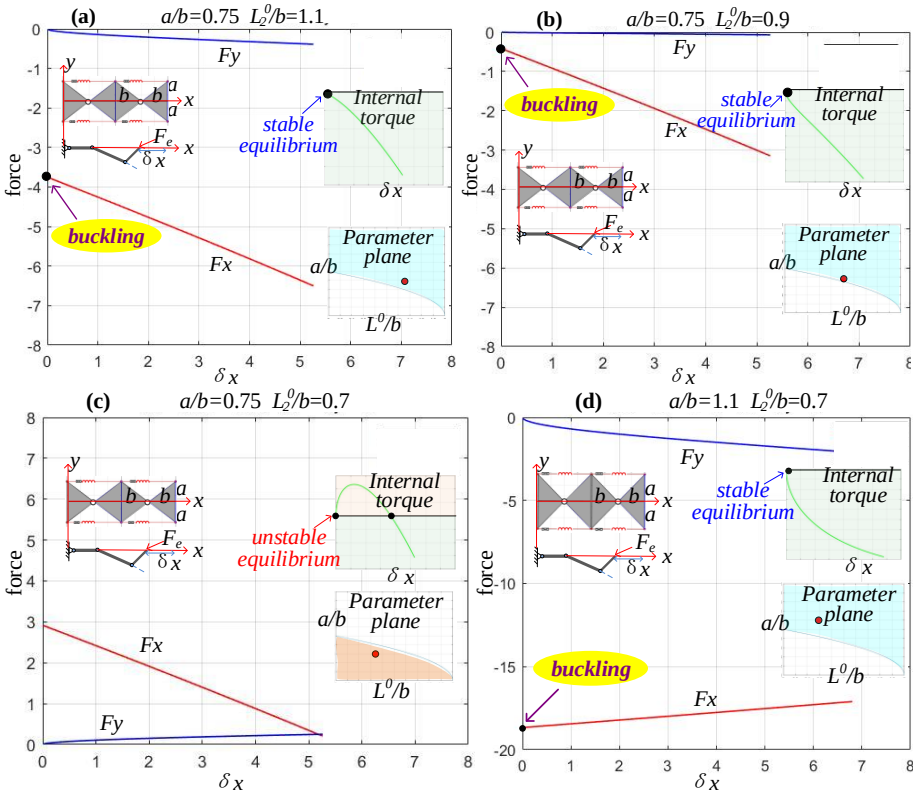

Figure 7: Force-deflection relations $F_x(\delta_x)$, $F_y(\delta_x)$ for different geometric parameters a, b, L^o

$$K_F = J_q^{-T} K_q J_q^{-1} \tag{35}$$

where

$$K_F = \begin{bmatrix} K_{Fxx} & K_{Fxy} \\ K_{Fyx} & K_{Fyy} \end{bmatrix} \tag{36}$$

Then, let us investigate variations of the mechanism stiffness coefficients while the control inputs L_{i1}^0 and L_{i2}^0 are different. Also, let us assume that both of the sections are controlled by a single input, i.e. $L_{11}^0 = var$, $L_{21}^0 = var$ and $L_{12}^0 = L_{22}^0$, which lead to the desired linear displacement $(\delta_x = var, \delta_y = 0)$. Corresponding simulation results are presented in Fig. 8, they demonstrate that the stiffness of the two-segment mechanism is very sensitive to its configuration. In particular, the mechanism stiffness is essentially reducing while the deflection δ_x is increasing.

It should be mentioned that, to have the stable equilibrium configuration, both two segments of the mechanism should satisfy the stability condition presented in the previous section. The latter is illustrated by Fig. 8c, where the right-hand side section of the mechanism is stable ($K_{q2} < 0$), but the left-hand side section is in unstable configuration ($K_{q1} > 0$). So the left hand side section moves until being stopped by the angle constrain. This shows if the control inputs (L_{i1}^0, L_{i2}^0) location is across the cusp of the parameter plan shown in Fig. 8c, the mechanism will be unstable also.

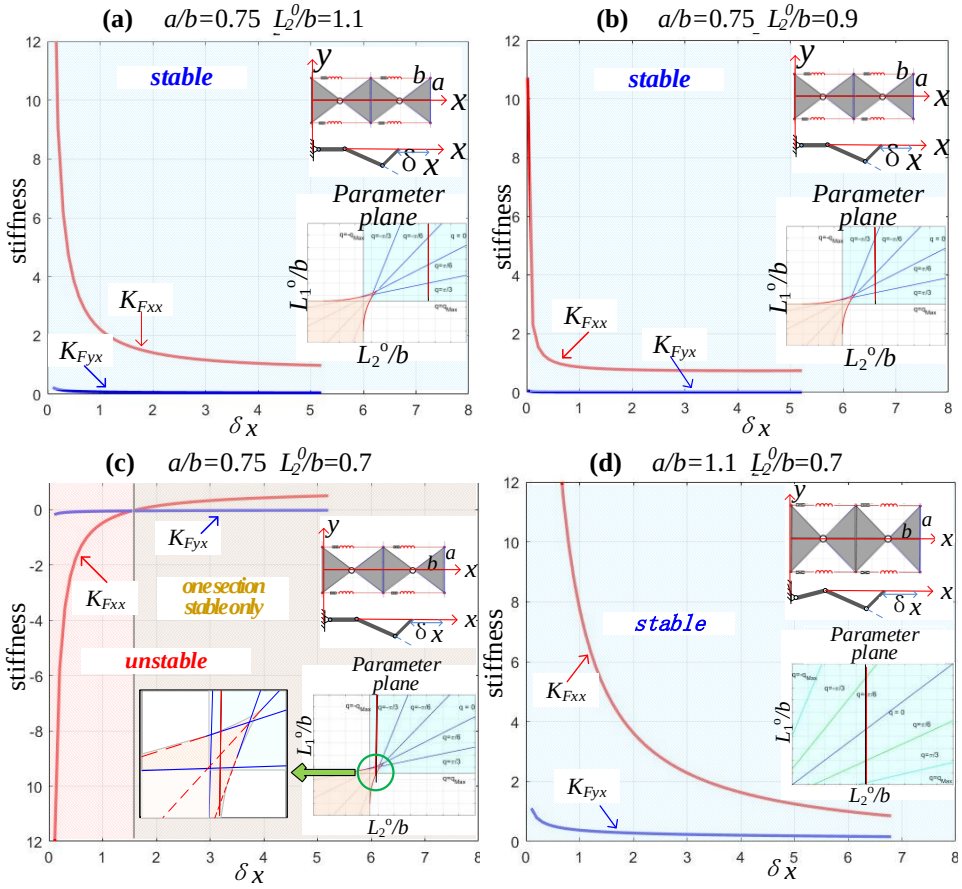

Figure 8: Stiffness coefficients for different geometric parameters (unloaded mode).

5 CONCLUSIONS

The paper presents some results on the stiffness analysis of a new type of tensegrity mechanism, which is composed of rigid triangles connected by passive joints. In contrast to conventional cable driven mechanisms, here there are two length-controllable elastic edges that can generate internal preloading. So, the mechanism can change its equilibrium configuration by adjusting the control inputs length. Such design is very promising and convenient for constructing a multi-section serial structures with high flexibility, which are needed in many modern robotic applications.

For one segment mechanism, the main attention was paid to a symmetrical structure composed of similar triangles. In particular, the case of equal control inputs was investigated in detail and analytical condition of equilibrium stability was obtained, which allows user to select the control inputs ensuring the mechanism controllability. The relation between the external torque and the deflection was also obtained allowing to find loaded equilibriums. It was proved that depending on parameters combinations, the actuation can lead to either the desired mechanism configuration (corresponding to a stable equilibrium) or undesired configuration corresponding to shifted stable equilibrium or joint limits. Besides, similar analysis has been done for the case of non-equal control inputs, and equivalent serial structure was proposed where the passive joint was replaced by a virtual actuated joint with variable stiffness. In future, these results will be used for the stiffness analysis of multi-section mechanisms that may demonstrate unusual behaviour under static load and suddenly change its configuration.

ACKNOWLEDGEMENTS

This work was supported by the China Scholarship Council (No. 201801810036).

REFERENCES

Rolf, M., & Steil, J. J. 2012. Constant curvature continuum kinematics as fast approximate model for the Bionic Handling Assistant. *2012 IEEE/RSJ International Conference on Intelligent Robots and Systems* (pp. 3440-3446). IEEE.

Yang, Y., & Zhang, W. 2015. An elephant-trunk manipulator with twisting flexional rods. *2015 IEEE International Conference on Robotics and Biomimetics (ROBIO)* (pp. 13-18). IEEE.

Skelton, R. E., & de Oliveira, M. C. 2009. *Tensegrity systems* (Vol. 1). New York: Springer.

Moored, K. W., Kemp, T. H., Houle, N. E., & Bart-Smith, H. 2011. Analytical predictions, optimization, and design of a tensegrity-based artificial pectoral fin. *International Journal of Solids and Structures*, *48*(22-23), 3142-3159.

Duffy, J., Rooney, J., Knight, B., & Crane III, C. D. 2000. A review of a family of self-deploying tensegrity structures with elastic ties. *Shock and Vibration Digest*, *32*(2), 100-106.

Arsenault, M., & Gosselin, C. M. 2006. Kinematic, static and dynamic analysis of a planar 2-DOF tensegrity mechanism. *Mechanism and Machine Theory*, *41*(9), 1072-1089.

Furet, M., Lettl, M., & Wenger, P. 2018. Kinematic analysis of planar tensegrity 2-X manipulators. *International Symposium on Advances in Robot Kinematics* (pp. 153-160). Springer, Cham.

Furet, M., & Wenger, P. 2018. Workspace and cuspidality analysis of a 2-X planar manipulator. *IFToMM Symposium on Mechanism Design for Robotics* (pp. 110-117). Springer, Cham.

Arsenault, M., & Gosselin, C. M. 2006. Kinematic, static and dynamic analysis of a planar 2-DOF tensegrity mechanism. *Mechanism and Machine Theory*, *41*(9), 1072-1089.

Wenger, P., & Chablat, D. 2018. Kinetostatic analysis and solution classification of a planar tensegrity mechanism. *Computational Kinematics* (pp. 422-431). Springer, Cham.

Moon, Y., Crane, C. D., & Roberts, R. G. 2012. Position and force analysis of a planar tensegrity-based compliant mechanism. *Journal of Mechanisms and Robotics*, *4*(1).

Venkateswaran, S., Furet, M., Chablat, D., & Wenger, P. 2019. Design and analysis of a tensegrity mechanism for a bio-inspired robot. *ASME 2019 International Design Engineering Technical Conferences and Computers and Information in Engineering Conference*. American Society of Mechanical Engineers Digital Collection.

Jones, R. M. (2006). Buckling of bars, plates, and shells. Bull Ridge Corporation.